Title
Bilayer-Structured Polymer Nanocomposites Exhibiting High Breakdown Strength and Energy Density via Interfacial Barrier Design

Journal
ACS Applied Energy Materials, 3(8)

ISSN
2574-0962

Authors
Li, He
Yao, Bin
Zhou, Yao
et al.

Publication Date
2020-08-24

DOI
10.1021/acsaem.0c01508

Peer reviewed

Bilayer-Structured Polymer Nanocomposites Exhibiting High Breakdown Strength and Energy Density via Interfacial Barrier Design

*He Li, Bin Yao, Yao Zhou, Wenhan Xu, Lulu Ren, Ding Ai and Qing Wang**

Department of Materials Science and Engineering, The Pennsylvania State University, University Park, Pennsylvania 16802, USA

*Email: wang@matse.psu.edu

ABSTRACT: The development of advanced dielectric materials with high breakdown strength, high dischargeable energy densities and great efficiencies is imperative to meet the ever-increasing demand of modern power systems and electronic devices. Herein, we present the layer-by-layer solution prepared bilayer-structured nanocomposite films with much enhanced capacitive performance via resolving the typical paradox between dielectric constant and breakdown strength in dielectric materials. The bilayered nanocomposite films are composed of Al_2O_3 dispersed in polystyrene as the interfacial barrier layer to inhibit electrical conduction and the polystyrene layer with TiO_2 to enhance dielectric constant. The resulting layered film exhibits a discharged energy density of 4.43 J/cm^3 along with ultrahigh charge–discharge efficiencies of > 90%, which is among the highest energy densities ever achieved in the polystyrene-based dielectric polymer nanocomposites. In addition, the composite films show outstanding cyclic stability under high electric fields, which would enable the long-term efficient operation of film capacitors. This

contribution represents an efficient route to high-energy-density dielectric composite materials using interfacial barrier architectures.

KEYWORDS: polymer nanocomposites, breakdown strength, energy density, bilayer structure, interfacial barrier

1. Introduction

The electrostatic capacitors possess the highest power density, lowest energy loss, a wide range of operating voltages and outstanding charge–discharge cyclability among the electrical energy storage devices including supercapacitors, electrolytic capacitors and lithium-ion batteries.[1–4] The electrostatic capacitors are one of the enabling technologies for advanced integrated electronics and electrical power systems. Compared with dielectric ceramics, polymer dielectrics display intrinsic advantages such as lightweight, flexibility, processability, and scalability.[5–10] Nevertheless, the low energy density owing to the low dielectric constant (k) of dielectric polymers leads to a large volume and weight of capacitor systems. For example, direct-current (DC) bus capacitors in the power inverters of hybrid electric vehicles can occupy ~35% of the inverter volume and ~23% of the converter weight.[3,11] Yet, the state-of-the-art biaxially oriented polypropylene (BOPP) film capacitors with a low k of ~2.2 merely delivers a discharged energy density (U_e) of less than 2.5 J/cm^3 even at a high electric field of 500 MV/m.[12,13] It is thus urgent to develop new dielectric polymers with improved energy densities to meet the ever-increasing demands in energy storage applications.

The working principle of an electrostatic capacitor involves the repetition of electrical polarization and depolarization processes on a dielectric material to electrostatically control charges on metallic electrodes.[2,14–16] For a linear dielectric material, the stored energy density U is governed by $U = 1/2\ DE^2 = 1/2\ k\varepsilon_0 E^2$, where D is the electric displacement, E is the applied electric field, and ε_0 is the permittivity of vacuum (8.85×10^{-12} F/m).[4,17] Therefore, U is significantly dependent on both D and E. Note that the E is limited by the breakdown strength of a dielectric material. In order to improve U, numerous efforts have been made to increase k using the composite approach based on high-k conductive filler such as carbon nanotubes (CNTs) and sliver nanowires,[4,18,19] as well as high-k ceramic filler such as titanium dioxide (TiO_2), barium titanate ($BaTiO_3$) and copper titanate calcium (CCTO) dispersed in organic matrices.[20–27] In spite of numerous breakthroughs, it is proven challenging to concomitantly retain low dielectric loss and high breakdown strength along with the improvement of k in the high-k polymer composites, which actually precludes a substantial increment in U.[28–31] On the other hand, the incorporation of wide-bandgap nanofiller with a moderate k (e.g., 8–20), e.g., aluminium oxide (Al_2O_3) and magnesium oxide (MgO), is found effective in impeding the leakage current and reducing energy loss without significant deteriorations in k and the breakdown strength of the polymer composites.[32–36] Moreover, compared to zero-dimensional (0-D) Al_2O_3 nanoparticles and one-dimensional (1-D) Al_2O_3 nanowires, it was verified that the parallelly arranged two-dimensional (2-D) Al_2O_3 nanoplates are capable of dispersing the applied electric field throughout the polymer matrix and preventing the propagation of breakdown channels, resulting in higher breakdown strength and smaller leakage current of the polymer nanocomposites.[36]

More recently, it has been corroborated experimentally and theoretically that the dielectric properties such as relaxation behavior and breakdown strength, as well as energy storage

performance of dielectric films, can be readily modulated by systematically varying the interfaces, chemical ratios, and structures of the constituent layers in the layered dielectric films.[37–40] The hierarchically arranged film structures could not only adjust the electric displacement and electric field distribution in dielectric materials at a macroscopic level but also integrate the intrinsic advantages of different dielectric components in each layer.[41–45] Xie *et al.*[46] manufactured linear/ferroelectric bilayer-heterostructured nanocomposites, in which ferroelectric polymer with dispersed $BaTiO_3$ nanoparticles provides a high *k* and linear polyimide is employed as an insulating interfacial barrier to assure high breakdown strength. Liu *et al.*[47] presented a symmetrical trilayer-structured nanocomposite based on the ferroelectric polymer matrix. The outer layers of the trilayered structure are doped with boron nitride nanosheets to impede charge transport and offer high breakdown strength, while the polymer matrix containing barium strontium titanate nanowires forms the central layer to process high *k* of the composites. A non-equilibrium layered structure for the dielectric composite film was designed by Wang *et al.*,[48] in which the ceramic fillers are gradient increased from the upper to bottom layers. It was found that the gradient electric fields formed at the interfaces between the adjacent layers act against the growth of breakdown channels. To further improve the breakdown strength, a barrier layer with a thickness of < 1 μm was added near the layer with the highest filler loading to block the charge injection. The aforementioned layer-structured polymer composites demonstrate the effectiveness of an electrically rigid barrier layer in enhancing breakdown strength and energy density. However, the currently reported multi-layered polymer composites are mainly centered on the ferroelectric polymer matrices represented by poly(vinylidene fluoride) (PVDF) and its copolymers and terpolymers.[4,38–48] Due to the inherent ferroelectric loss and large remnant polarization, the charge–discharge efficiency (η) described in ferroelectric polymers usually ranges from 50 - 80%, which

signifies that a notable portion of the stored electrical energy in the charging process could not be recovered via discharging but is dissipated in the form of Joule heat.[7,15,16] Compared with the PVDF-based ferroelectric polymers, linear polystyrene (PS) exhibits much low loss, which would assure high η of the polymer nanocomposites. Additionally, PS has desirable solution processability and a larger k relative to PP (~2.75 versus ~2.2), which would enable facile preparation of dielectric with potential high energy densities.

In this work, we describe PS-based bilayered composite films fabricated through a cost-effective solution approach. The barrier layer is functionalized with highly insulating 2-D Al_2O_3 fillers to withstand electrical conduction and provide high breakdown strength, whereas the high-k layer from PS/TiO_2 is designated to improve electric displacement of the polymer composite. A simultaneous enhancement in both k and breakdown strength, along with a reduction in dielectric loss have been achieved in the bilayered nanocomposite films. The layered composite exhibits superior energy storage performances as well as outstanding high-field cyclic stability.

2. Materials and Methods

2.1 Materials fabrication

N, *N*-dimethylformamide (DMF) solvent of 99.8% purity was purchased from Sigma-Aldrich. TiO_2 (rutile) nanoparticles with an average diameter of 30 nm were purchased from US Research Nanomaterials. Al_2O_3 nanoplates were prepared from $Al_2(SO_4)_3 \cdot 18H_2O$ powders (Sigma-Aldrich) using a modified hydrothermal reaction method.[36,49] Commercial BOPP film for cyclic tests was provided by PolyK Tech., USA. PS powders with an average molecular weight of 280000 were purchased from Sigma-Aldrich.

The schematic fabrication of the single-layered PS/TiO_2 composites and the bilayered PS/TiO_2/Al_2O_3 composites are shown in **Figure 1**(a). To obtain the single-layered polymer nanocomposite films, PS powders were first dissolved in DMF solvent using magnetic stirring for more than 12 h to yield transparent solution, which is marked as Solution **1**. After then, an appropriate amount of TiO_2 nanoparticles were introduced into DMF and designated as Solution **2**. Solution **2** was sonicated by using a water bath ultrasonics (250 W) for more than 4 h before mixing with Solution **1**. The mixture of Solution **1** and **2** was solution casted onto a flat glass substrate at 60 ^oC and vacuum dried for more than 4 h. Accordingly, the bilayered polymer nanocomposites were achieved via a facile layer-by-layer solution casting approach. An appropriate amount of Al_2O_3 nanoplates were mixed with DMF and designated as Solution **3**. Solution **3** was sonicated by using water bath ultrasonics (250 W) for more than 4 h before mixing with Solution **1**. The mixture of Solution **1** and **3** was solution casted onto the surface of PS/TiO_2 films at 60 ^oC and vacuum dried for more than 4 h. For the series of the bilayered films investigated hereafter, the thickness ratio of the PS/TiO_2 layer to the PS/Al_2O_3 layer was fixed to ~2:1 to simplify the experimental variables. The single-layered PS/TiO_2 films and the bilayered PS/TiO_2/Al_2O_3 films were peeled off after soaking in water for a few seconds. The single-layered films are termed as PS/TiO_2-*x*, and the bilayered PS/TiO_2/Al_2O_3 films are named as PS/TiO_2-*x*/Al_2O_3-*y*, where *x* and *y* stand for the volume fraction of TiO_2 nanoparticles and Al_2O_3 nanoplates in PS matrix, respectively. The thickness of the resulting composite films was within the range of 12 ± 2 μm.

2.2 Instrumentation and characterization

Scanning electron microscope (SEM) images were obtained on a ZEISS EVO10 equipment. The surface of Al_2O_3 nanofiller and polymeric film samples were sputter coated with ultrathin gold

layers prior to observation. Transmission electron microscope (TEM) images were achieved using a FEI JEM-F200 equipment. Prior to observation, TiO_2 nanoparticles were sonicated in acetone to yield a clear solution, and a few drops of the solution were dropped onto a lacey carbon covered copper grid. The element mapping images of Al_2O_3 nanoplate were achieved using an energy dispersive spectroscopy (EDS) attached to TEM. Fourier transform infrared (FTIR) spectra were recorded by a Varian Digilab FTS-8010 spectrometer in the transmission mode. The TiO_2 and Al_2O_3 nanofillers were mixed with potassium bromide (KBr) and pressed into pellets. Dielectric breakdown strength measurements were performed using a Trek P0621P amplifier based on an electrostatic pull-down testing method under a DC voltage ramp of 500 V/s. At least 15 measurements were conducted for the statistical analysis. Frequency-dependent dielectric spectra were recorded using a Hewlett Packard 4284A LCR meter within the frequency range of 10^2 to 10^6 Hz. High field electric displacement–electric field (*D*–*E*) loops including the cyclic tests were collected using a modified Sawyer-Tower circuit under a triangular unipolar wave with a frequency of 10 Hz. Leakage current densities were collected by a Hewlett Packard 4140B pA meter with Trek 1010BHS amplifier as a high-voltage source in conjunction with a Delta Design 9023 oven under an applied DC voltage of 200 MV/m. For all the electrical measurements, gold electrodes with a thickness of ~60 nm were sputtered onto both sides of the polymer and polymer nanocomposite film samples. Fast discharge tests were carried out based on a high voltage metal oxide semiconductor field effect transistor (MOSFET) switch (Behlke HTS81) with a typical discharging time of 10 μs. The resistance of the load resistor was selected as 6.5 kΩ. In order to prevent creeping discharge in the air atmosphere, the dielectric breakdown strength, *D*–*E* loop and fast discharge measurements were conducted in a Galden HT insulation fluid.

3. Results and Discussion

3.1 Microstructure characterization

The morphologies of 0-D TiO_2 nanoparticles and 2-D Al_2O_3 nanoplates are shown in **Figures 1**(b) and 1(c), respectively. The average diameter of the TiO_2 nanoparticles is 30 nm. The Al_2O_3 nanoplates are in a hexagonal shape with a thickness of 20-30 nm and a width of 800-1000 nm. The element mappings of aluminum and oxygen of a Al_2O_3 nanoplate are obtained using EDS and demonstrated in **Figure S1** (Supporting Information). **Figures 1**(d) and 1(e) show the representative SEM images of the cross-section of the single-layered PS/TiO_2-2 and the bilayered PS/TiO_2-2/Al_2O_3-5 nanocomposite films. Both inorganic fillers of TiO_2 and Al_2O_3 are well dispersed in the PS matrix, which is presumably attributed to the polar -OH groups (**Figure S2**, Supporting Information) on the surface of inorganic oxides that endow the homogenous dispersion of nanofillers in polar solvent (e.g., DMF) during the solution fabricating processes. The distinct double-layered structure fabricated from a layer-by-layer solution casting method can be visually observed (**Figure 1**(e)). The thicknesses of the PS/TiO_2 and PS/Al_2O_3 layers can be simply and precisely controlled by adjusting the concentration of Solutions **1**, **2**, and **3**. Notably, the barrier layer (PS/Al_2O_3) and the bottom layer (PS/TiO_2) in the bilayered composite film demonstrates a clearly demarcated but defect-free interfacial structure. The tightly bonded interface between two adjacent layers is desirable as it would assure the high dielectric strength of the polymer nanocomposites.

3.2 Dielectric breakdown and dielectric spectra

To determine the optimized volume fraction of TiO_2 nanoparticles in the PS/TiO_2 layer, the dielectric breakdown strength of single-layer PS/TiO_2 nanocomposites was first analyzed according to a two-parameter Weibull statistic

$$P(E) = 1 - \exp(-(E/\alpha)^{\beta}) \quad (1)$$

where $P(E)$ is the cumulative probability of electric failure, E is the experimental result of breakdown strength, α is the scale parameter which corresponds to the breakdown strength at a cumulative failure probability of ~63.2% and regarded as Weibull breakdown strength (E_b) and β is the shape parameter which refers to the scatter of the experimental data. A large β value signifies a narrow distribution of data, representing high dielectric reliability. The Weibull distribution plots of pristine PS and the PS/TiO_2 nanocomposites are shown in **Figure 2**(a), and the corresponding Weibull distribution parameters derived from the fitted plots are summarized in **Table 1**.

Compared with the polymer matrix, slight enhancement of E_b and β are found in the single-layered PS nanocomposites with relatively low TiO_2 loadings (i.e., ≤ 2 vol%). The improvement in dielectric strength and reliability could be attributed to the formation of the organic/inorganic interfaces in the composites, which serve as effective trapping centers and electron scatters to hamper carrier transportation in the dielectric materials.[33,50] However, it is noteworthy that the difference in k between inorganic filler and organic phase (e.g., ≥ 40 of TiO_2 versus ~2.7 of PS, at 10^3 Hz) would lead to electric field distortion in the polymer composites.[51,52] With further increasing filler content, the TiO_2 nanoparticles may create a more significant distortion of local electric fields and yield a reduced E_b as well as lead to the degradation of dielectric reliability. The optimized filler loading of 2 vol% is thus chosen for the PS/TiO_2 layer as a result of the greatest E_b value of 415.64 MV/m and the largest β value of 14.97 among the single-layered composite films, which is about 6.8% higher than that of unfilled PS (389.09 MV/m). Subsequently, the influence of the interfacial barrier layer on the dielectric breakdown strength is revealed based on the PS-TiO_2-2 nanocomposites, as shown in **Figure 2**(b) and **Table 1**. The incorporated wide bandgap Al_2O_3 nanoplates in the barrier layer could not only provide higher resistance to the

conduction processes than TiO_2 nanoparticles, but also are more efficient in preventing the propagation of electrical trees across the nanocomposites due to the high aspect ratio 2-D structure. Moreover, the barrier layer would regulate the electric field distribution in dielectric films at a macroscopic level.[38] Owing to a lower k of Al_2O_3 (9–10) relative to TiO_2, which is closer to that of the polymer matrix, the electric field distortion in the PS/TiO_2 layer could be sufficiently alleviated. As expected, a concurrent improvement in E_b and β is obtained in the bilayered PS/TiO_2/Al_2O_3 nanocomposites, both of which are maximized at 543.43 MV/m and 17.84 of the bilayered nanocomposite with a 5 vol% Al_2O_3-filled barrier layer. The ~40% increment of characteristic breakdown strength, as well as the largely improved dielectric reliability of the bilayered composite compared to pristine polymer, would enable the efficient operation of film capacitors under high electric fields to achieve high energy densities.

In addition to dielectric breakdown strength, k is another critical metric of dielectric materials for dielectric energy storage applications. The frequency dependence of k and loss tangent (tanδ) of pristine PS and single-layered PS/TiO_2 nanocomposites are shown in **Figure 3**(a). **Figure 3**(b) depicts the variations of k and tanδ (at 10^3 Hz) of the PS nanocomposites with the TiO_2 filler content. Apparently, the k of the nanocomposites increases monotonically with the increase of TiO_2 loading, e.g., at 10^3 Hz, from 2.72 of pristine PS to 3.1 of the nanocomposite filled with 4 vol% TiO_2 nanoparticles as a consequence of higher k of TiO_2 filler with respect to the PS matrix. However, it is commonly accepted that the high-k approach to increase the k of polymer composites is usually accompanied with the increase of dielectric loss and the decrease of dielectric breakdown strength when compared with the polymer matrix. As described in **Figure 3**(b), the single-layered PS nanocomposites consisting of a small amount of TiO_2 (i.e., $\leq$ 2 vol%) could retain the distinct low tan δ of the polymer matrix (e.g., < 0.007 at 10^3 Hz), whereas the tanδ

of the composites increases constantly with the further increase of TiO_2 filler content. This trend matches well with the variations in the E_b value of the single-layered composites obtained from Weibull statistic (**Table 1**) and reaffirms the rationality of the designated optimal filler loading (i.e., 2 vol%) of the PS/TiO_2 layer. **Figure 3**(c) describes the frequency dependence of k and tanδ of pristine PS and the PS/TiO_2-2-based bilayered nanocomposites. The variations of k and tanδ (at 10^3 Hz) of the PS/TiO_2-2-based composites with the Al_2O_3 filler content are revealed in **Figure 3**(d). The k of the bilayered nanocomposites containing the barrier layer with a small amount of Al_2O_3 fillers (i.e., PS/TiO_2-2/Al_2O_3-1) is much lower than the single-layered PS/TiO_2-2 nanocomposite. While the k increases steadily with increasing Al_2O_3 content in the barrier layer, e.g., at 10^3 Hz, from 2.86 of the PS/TiO_2-2/Al_2O_3-1 nanocomposite to 2.93 and 2.95 of the PS/TiO_2-2/Al_2O_3-5 and the PS/TiO_2-2/Al_2O_3-7 nanocomposites, representing a 7.7% and 8.5% increment compared with PS matrix, respectively. Moreover, it is of interest to note that the tanδ of the bilayered nanocomposites decreases gradually with the increase of Al_2O_3 content, and maintains relatively low values of ~0.0045 (at 10^3 Hz) for the PS/TiO_2-2/Al_2O_3-5 and the PS/TiO_2-2/Al_2O_3-7 nanocomposites. As the PS/TiO_2-2/Al_2O_3-5 nanocomposite exhibits much higher E_b value when compared to the PS/TiO_2-2/Al_2O_3-7 nanocomposite (543.43 MV/m versus 501.61 MV/m), a Al_2O_3 loading of 5 vol% was thus chosen in the barrier layer hereafter to investigate the energy storage performance of the polymer composites.

3.3 Energy storage performance

The D–E loops obtained from the modified Sawyer-Tower circuit under a unipolar wave have been used to evaluate the energy storage performance of the PS-based dielectric materials. **Figure S3** (supporting Information) describes a schematic D–E loop of linear dielectric material. The discharged energy density (U_e) can be obtained by the integration of the area between the

discharging curve and D axis. The energy loss (U_l) is represented by the area bounded by the charging curve, discharging curve and D axis. A series of D–E loops of pristine PS, single-layered PS/TiO_2-2, and bilayered PS/TiO_2-2/Al_2O_3-5 are shown in **Figure S4** (supporting Information). As compared in **Figure 4**(a), the higher k of the incorporated inorganic fillers gives rise to a larger D of the dielectric material, e.g., 0.011 C/m^2 of the polymer matrix and 0.0126 C/m^2 of the bilayered nanocomposite, at 400 MV/m. **Figure 4**(b) shows the U_e of the dielectric polymer and polymer nanocomposites measured at varied electric fields, in which the dashed curve describes the performance of the commercially available BOPP. Owing to the larger k, the PS-based dielectric materials exhibit higher U_e than BOPP at the same fields. For example, at an applied electric field of 200 MV/m, which is the operating condition of film capacitors in the hybrid electric vehicle, the bilayered nanocomposite delivers a U_e of 0.6 J/cm^3, signifying a ~55% improvement when compared to BOPP (0.39 J/cm^3). Moreover, the barrier layer provides the PS-based composites higher resistance to dielectric breakdown, which gives rise to a significantly enhanced maximum electric displacement (D_{max}) of 0.018 C/m^2 and an optimized U_e of 4.43 J/cm^3 at 550 MV/m of the bilayered PS/TiO_2-2/Al_2O_3-5 nanocomposite. Accordingly, the charge–discharge efficiency (η), which is another pivotal parameter in determining the energy storage capability of a dielectric material, can be derived from the equation

$$\eta = U_e / (U_e + U_l) \times 100\% \quad (2)$$

As seen in **Figure 4**(c), the single-layered nanocomposites containing high-k TiO_2 nanoparticles exhibit a marked reduction in η in comparison with pristine PS. In contrast, the embedded Al_2O_3 nanoplates in the barrier layer effectively inhibit the dissipation of energy of the bilayered nanocomposite and retain the distinct high η of PS matrix. Consequently, the bilayered PS/TiO_2-2/Al_2O_3-5 nanocomposite maintains a η >90% even at an ultrahigh electric field of 500

MV/m. As summarized in **Figure 4**(d), the concurrently improved dielectric parameters including k, E_b and D_{max} endows the greater capacitive energy storage performance of the bilayered PS/TiO_2-2/Al_2O_3-5 nanocomposite compared to pristine PS and single-layered PS/TiO_2-2 nanocomposite. Remarkably, the U_e of 4.43 J/cm^3 obtained in the bilayered nanocomposite, is not only ~112% and ~71% greater than pristine polymer (2.09 J/cm^3) and the single-layered nanocomposite (2.59 J/cm^3) but also among the best of the nanocomposites based on linear polymer matrices (e.g., 3.86 J/cm^3 of PP-based and 4.1 J/cm^3 in PS-based nanocomposite) reported so far (**Figure 4**(e)).[22,29–32,53–56] To evaluate the discharge rate of the polymer nanocomposite, fast discharge test has been conducted using a typical high-speed capacitor circuit at identical resistor-capacitor (RC) time constant. The power density (P) of dielectric materials is derived from the following equation

$$P = U_{95\%} / t_{95\%} \quad (3)$$

where the $t_{95\%}$ is the discharge time defined as the time for the dischargeable energy in a load resistor to reach 95% of the total value, and the $U_{95\%}$ is the discharged energy density recorded at the $t_{95\%}$. As compared in **Figure S5** (Supporting Information), the bilayered PS/TiO_2-2/Al_2O_3-5 nanocomposite is able to release 95% of the stored energy at a rate of 1.51 μs, whereas the corresponding discharge time of BOPP is 1.47 μs, at 200 MV/m. Accordingly, a more than 40% increment is obtained in the bilayered nanocomposite in comparison with the commercially available film capacitor, e.g, 0.347 MW/cm^3 of PS/TiO_2/Al_2O_3 nanocomposite versus 0.245 MW/cm^3 of BOPP.

3.4 Electrical conduction

It is well-recognized that the energy loss (i.e., reduction in η), especially under the high fields, is dominated by electrical conduction. The energy loss of capacitors is dissipated in the form of leakage current and would generate Joule heat and reduce the lifespan of dielectric

capacitors. **Figure S6** (supporting Information) compares the leakage current density of the bilayered PS/TiO_2-2/Al_2O_3-5 nanocomposite with the corresponding single-layered PS/TiO_2-2 nanocomposite and pristine PS. Evidently, the bilayered nanocomposite have the lowest leakage current density that is nearly one order magnitude lower than the single-layered PS/TiO_2-2 nanocomposite, e.g., 3.31×10^{-12} A/cm^2 versus 2.95×10^{-11} A/cm^2 measured under an applied electric field of 200 MV/m. According to the Arrhenius relationship, conduction activation energy (A_c) is given as

$$\sigma(T) = \sigma_0 \times \exp(-A_c e / K_b T) \quad (4)$$

where σ is the volume electric conductivity calculated from leakage current density, σ_0 is a prefactor, e is the charge of the carriers, K_b is the Boltzmann constant, and T is the temperature in Kelvin. As shown in **Figure 5**, A_c determined from Equation (3) are 0.75 eV, 0.71 eV and 0.92 eV for pristine PS, the single-layered PS/TiO_2 nanocomposite and the bilayered PS/TiO_2/Al_2O_3 nanocomposite, respectively. A large A_c represents a higher potential energy barrier that needs to be overcome to proceed with conduction process, which is in concert with a small current density observed in the bilayered nanocomposite containing wide-bandgap Al_2O_3 fillers (e.g., 7.2–8.8 eV).[33,36] On the contrary, the presence of TiO_2 decreases the energy barrier of the organic phase due to its inherent electronic structure with a much narrower bandgap (e.g., 3–3.5 eV of TiO_2 versus 4.8–5 eV of PS matrix).[33,57,58] The pronounced decrease in the current density along with the largest activation energy are strong indications that the 2D Al_2O_3-doped layer is efficient in acting as reticular barriers against charge injection from electrodes as well as inhibiting charge transport in the polymer composites, which again accounts for the enhanced dielectric breakdown strength and increased η of the bilayered nanocomposite.

3.5 High-field cyclability

The cyclic charging–discharging measurements have been employed to examine the stability of the bilayered PS/TiO_2-2/Al_2O_3-5 nanocomposite film under high electric fields (e.g., 200 MV/m). The corresponding U_e values of the bilayered nanocomposite and commercially available BOPP over a 5000-cycle of charging–discharging are shown in **Figure 6**. It is clear that the bilayered nanocomposite film exhibits excellent cyclability, which is comparable to the BOPP film. To further quantifiably evaluate the high-field stability of the dielectric materials, the change rate of discharged energy density (R_c) is described as

$$R_c = |(U_{ei} - U_{e1}) / U_{e1}| \quad (5)$$

where U_{e1} is the U_e of the first charging–discharging cycle, and U_{ei} is the U_e obtained from the i^{th} cycle (i stands for the number of cycles). Remarkably, while both dielectric films deliver variations in experimental data of < 2% throughout the whole cycle range (**Figure S7**, supporting Information), the bilayered nanocomposite even processes lower extremum of R_c than the state-of-the-art commercial BOPP, e.g., 1.44% versus 1.65%, manifesting its superior stability for the high-field applications.

4. Conclusions

In summary, we have presented a facile approach to the bilayered PS-based nanocomposite films consisting of an interfacial barrier layer with high insulation strength and the high-k PS/TiO_2 layer. The distinct topological structure has been imaged by electron microscopy, and the structure–electrical property correlations have been systematically investigated. The designed barrier layer is found to be efficient in reducing dielectric loss as well as providing high resistance to electrical conduction and dielectric breakdown. Consequently, a high discharged energy density of 4.43 J/cm^3 along with outstanding charge–discharge efficiencies (e.g., 93% at 500 MV/m) has

been obtained in the bilayered PS/TiO_2/Al_2O_3 nanocomposite film with the experimentally optimized microstructure, which far exceeds the current linear dielectric-based nanocomposites. Outstanding dielectric cyclability has also been corroborated in the bilayered nanocomposite under high electric fields. This work demonstrates that by designing the spatial organization of fillers with different electrical and dielectric properties in the layered polymer composites, one can significantly enhance the capacitive performance by using low-cost commodity polymers.

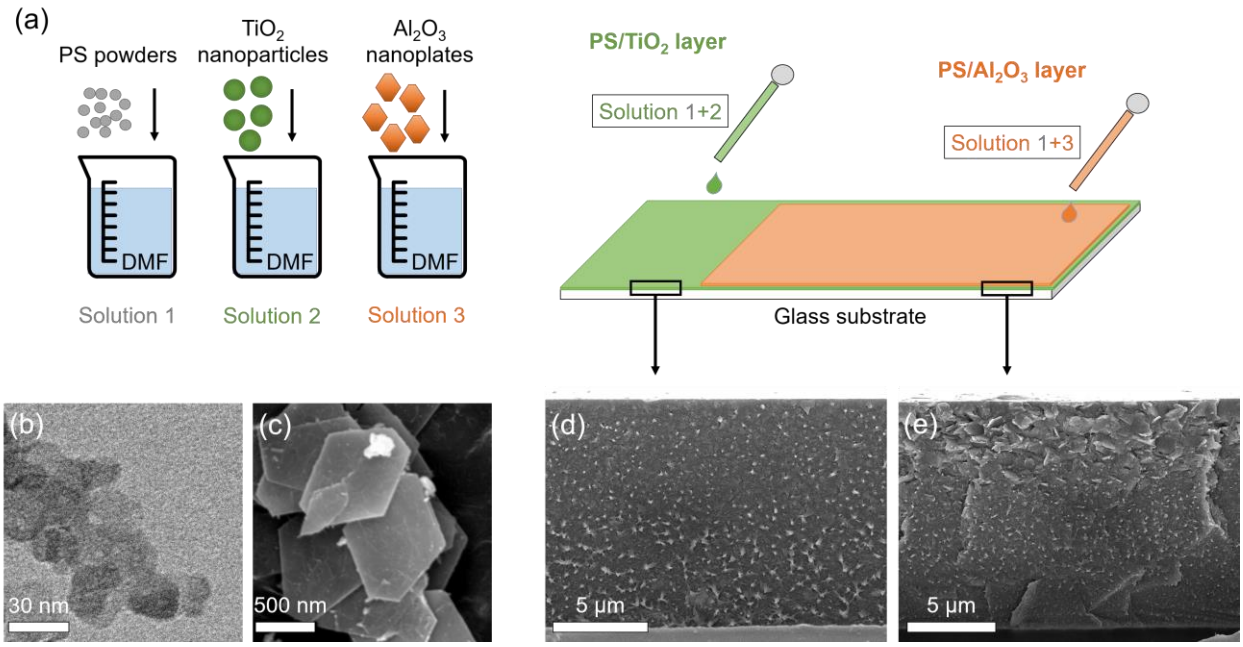

Figure 1. (a) Schematic of the single-layered PS/TiO_2 composites and the bilayered PS/TiO_2/Al_2O_3 composites. (b) TEM image of TiO_2 nanoparticles. (c) SEM image of Al_2O_3 nanoplates. (d) Cross-sectional image of the single-layered composite with 2 vol% TiO_2. (e) Cross-sectional image of the bilayered composite with 2 vol% TiO_2 and 5 vol% Al_2O_3.

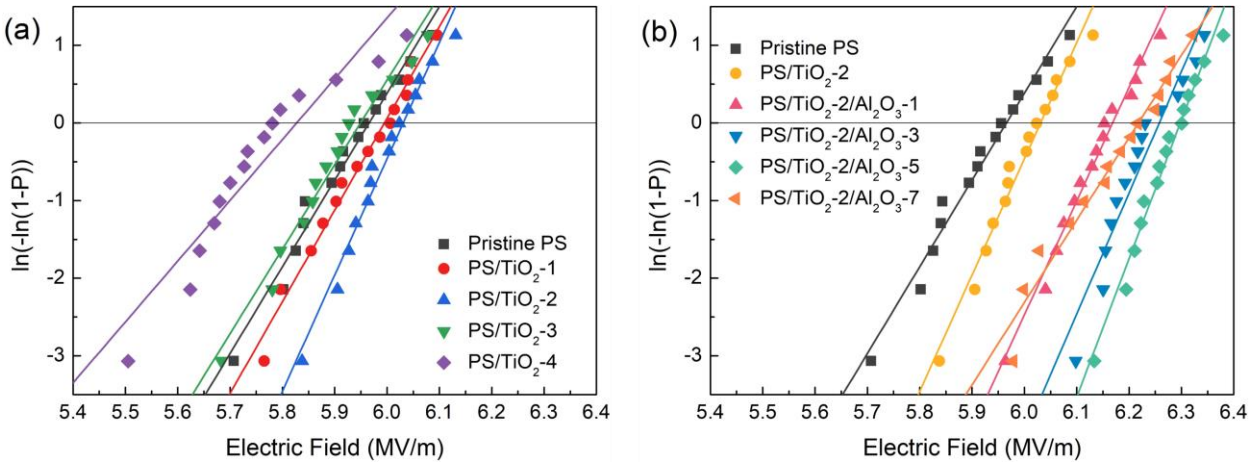

Figure 2. Weibull distribution plots of pristine PS and (a) Single-layered PS/TiO_2 nanocomposites, (b) Bilayered PS/TiO_2/Al_2O_3 nanocomposites.

Table 1. Weibull distribution parameters of pristine PS, single-layered PS/TiO_2 nanocomposites, and bilayered PS/TiO_2/Al_2O_3 nanocomposites.

	Sample	E_b **(MV/m)**	β
Polymer matrix	Pristine PS	389.09	11.17
Single-layer composites	PS/TiO_2-1	401.62	11.81
	PS/TiO_2-2	415.64	14.97
	PS/TiO_2-3	383.68	10.89
	PS/TiO_2-4	339.47	7.83
Bilayered composites	PS/TiO_2-2/Al_2O_3-1	478.04	14.66
	PS/TiO_2-2/Al_2O_3-3	522.12	15.61
	PS/TiO_2-2/Al_2O_3-5	543.43	17.84
	PS/TiO_2-2/Al_2O_3-7	501.61	10.61

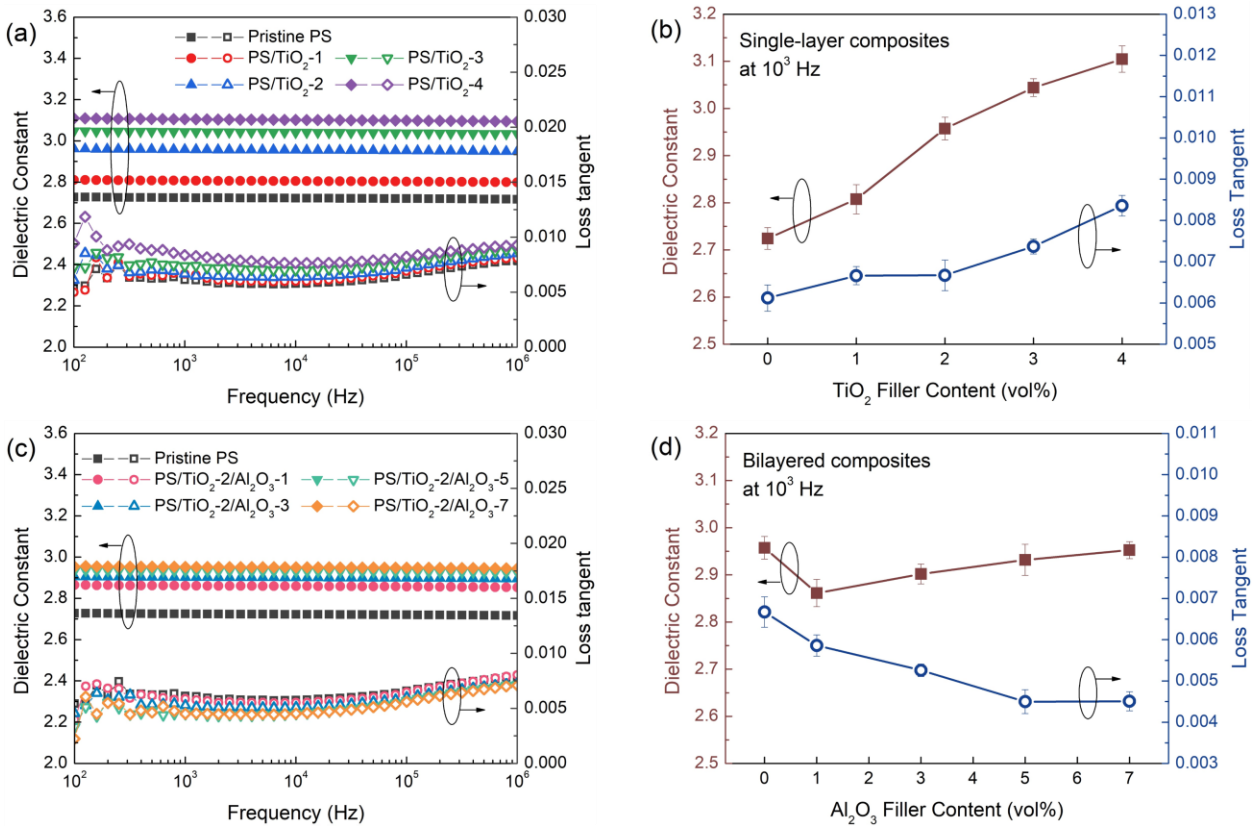

Figure 3. Frequency dependence of the dielectric constant (k) and loss tangent (tan δ) of pristine PS, (a) Single-layered PS/TiO_2 nanocomposites, and (c) Bilayered PS/TiO_2/Al_2O_3 nanocomposites. k and tanδ at 10^3 Hz of pristine PS, (b) Single-layered PS/TiO_2 nanocomposites as a function of TiO_2 content, and (d) Bilayered PS/TiO_2/Al_2O_3 nanocomposites with 2 vol% TiO_2 as a function of Al_2O_3 content.

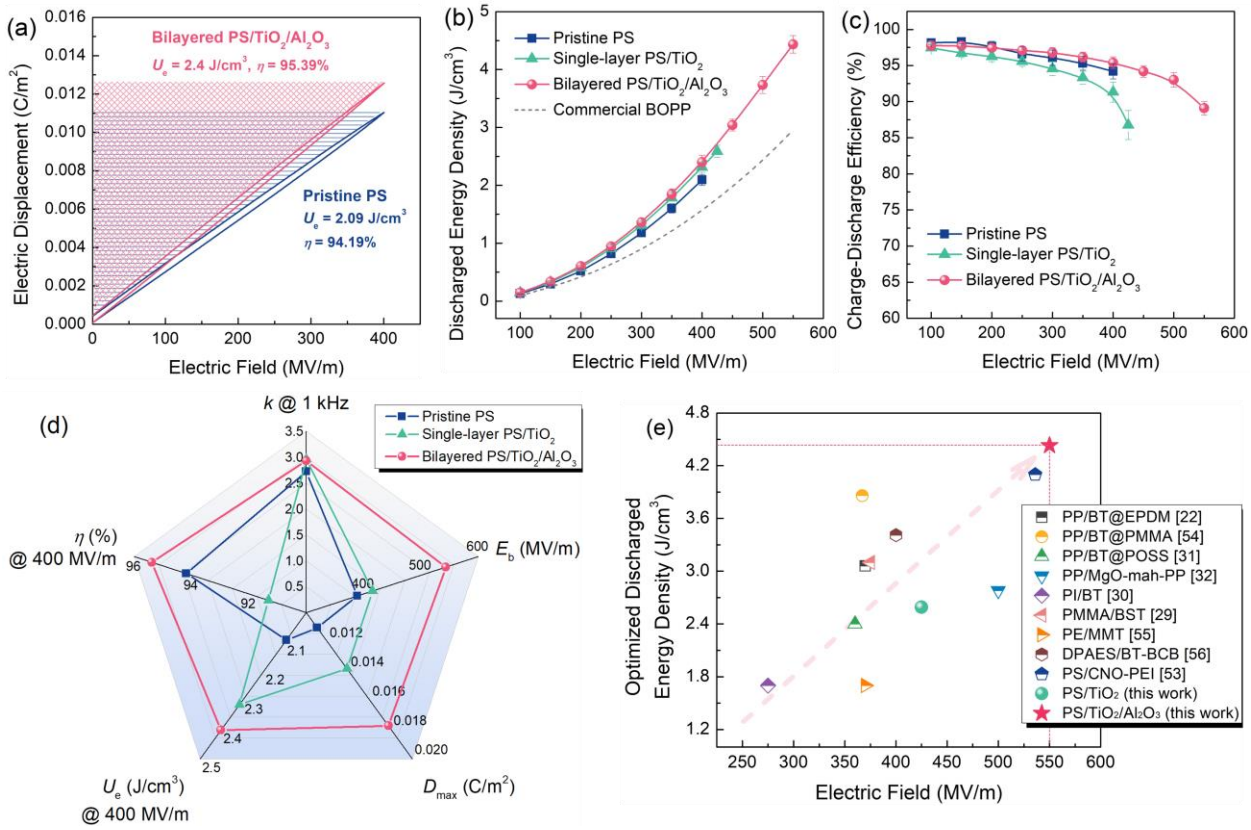

Figure 4. (a) *D–E* loops of pristine PS and bilayered PS/TiO_2-2/Al_2O_3-5 nanocomposite at 400 MV/m. (b) U_e of pristine PS, BOPP, single-layered PS/TiO_2-2 nanocomposite, and bilayered PS/TiO_2-2/Al_2O_3-5 nanocomposite. BOPP data is derived from our previous work.[12] (c) η of pristine PS, single-layered PS/TiO_2-2 nanocomposite, and bilayered PS/TiO_2-2/Al_2O_3-5 nanocomposite. (d) Comparison of k, E_b, D_{max}, U_e and η among pristine PS, single-layered PS/TiO_2-2 nanocomposite, and bilayered PS/TiO_2-2/Al_2O_3-5 nanocomposite. (e) Comparison of U_e of the reported nanocomposites based on linear polymer matrices. The reference polymer composites are PP filled with ethylene propylene diene monomer coated $BaTiO_3$ (PP/BT@EPDM),[22] PP filled with poly(methyl methacrylate) coated $BaTiO_3$ (PP/BT@PMMA),[54] PP filled with polyhedral oligomeric silsesquioxane coated $BaTiO_3$ (PP/BT@POSS),[31] PP filled

with PP-graft-maleic anhydride modified MgO (PP/MgO-mah-PP),[32] polyimide filled with $BaTiO_3$ nanoparticles (PI/BT),[30] poly(methyl methacrylate) filled with $Ba_{0.5}Sr_{0.5}TiO_3$ nanoparticles (PMMA/BST),[29] polyethylene filled with organomontmorillonite (PE/MMT),[55] poly(arylene ether sulfone)-containing side propenyl groups (DPAES) filled with benzocyclobutene modified $BaTiO_3$ (DPAES/BT-BCB),[56] PS filled with polyethyleneimine modified $Ca_2Nb_3O_{10}$ nanosheets (PS/CNO-PEI).[53]

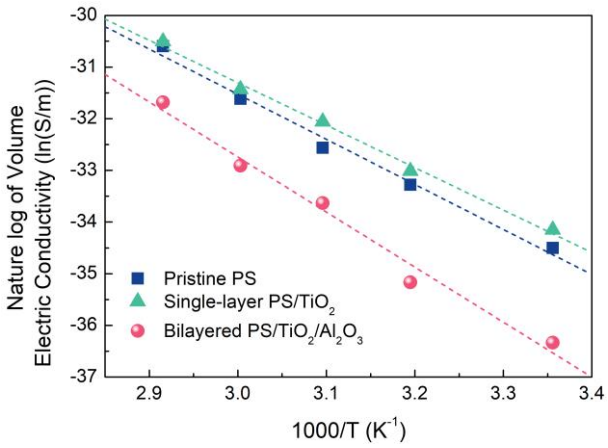

Figure 5. Arrhenius plots of volume conductivity of pristine PS, single-layered PS/TiO_2-2 nanocomposite, and bilayered PS/TiO_2-2/Al_2O_3-5 nanocomposite measured at 200 MV/m.

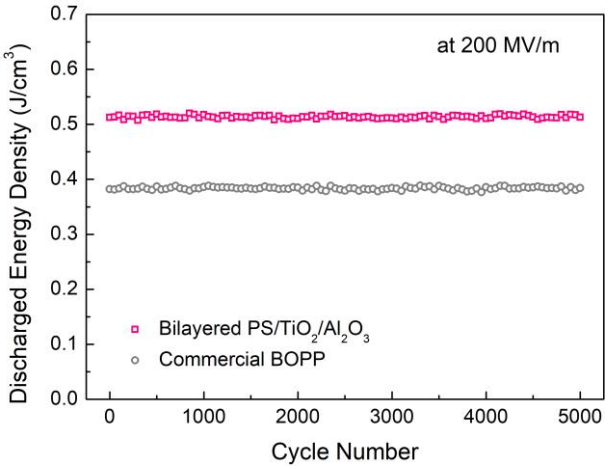

Figure 6. U_e derived from 5,000 charging–discharging cycles of BOPP and bilayered PS/TiO_2-2/Al_2O_3-5 nanocomposite measured at 200 MV/m.

ASSOCIATED CONTENT

Supporting Information. The Supporting Information is available free of charge on the ACS Publications website. FTIR spectra of TiO_2 nanoparticles and Al_2O_3 nanoplates. Element mapping of aluminum and oxygen of Al_2O_3 nanoplate. Schematic electric displacement–electric field (*D*–*E*) loop of a linear dielectric material. *D*–*E* loops of pristine PS, single-layered PS/TiO_2 nanocomposite, and bilayered PS/TiO_2/Al_2O_3 nanocomposite. Discharged energy density as a function of time of BOPP and the bilayered PS/TiO_2/Al_2O_3 nanocomposite. Leakage current of pristine PS, single-layered PS/TiO_2 nanocomposite, and bilayered PS/TiO_2/Al_2O_3 nanocomposite. Change rate of discharged energy density BOPP and the bilayered PS/TiO_2/Al_2O_3 nanocomposite.

AUTHOR INFORMATION

Corresponding Author

* wang@matse.psu.edu (Q. Wang)

NOTES

The authors declare no competing financial interest.

ACKNOWLEDGMENT

The authors acknowledge the support from the US Office of Naval Research.

REFERENCES

(1) Sarjeant, W. Capacitors. *IEEE Trans. Electr. Insul.* **1990**, *25*, 861-922.

(2) Chu, B.; Zhou, X.; Ren, K.; Neese, B.; Lin, M.; Wang, Q.; Bauer, F.; Zhang, Q. M. A dielectric polymer with high electric energy density and fast discharge speed. *Science* **2006**, *313*, 334-336.

(3) Li, H.; Gadinski, M.R.; Huang, Y.; Ren, L.; Zhou, Y.; Ai, D.; Han, Z.; Yao, B.; Wang, Q. Crosslinked fluoropolymers exhibiting superior high-temperature energy density and charge–discharge efficiency. *Energy Environ. Sci.* **2020**, *13*, 1279-1286.

(4) Li, H.; Liu, F.; Fan, B.; Ai, D., Peng, Z.; Wang, Q. Nanostructured ferroelectric-polymer composites for capacitive energy storage. *Small Methods* **2018**, *2*, 1700399.

(5) Huang, X.; Sun, B.; Zhu, Y.; Li, S.; Jiang, P. High-*k* polymer nanocomposites with 1D filler for dielectric and energy storage applications. *Prog. Mater. Sci.* **2019**, *100*, 187-225.

(6) Luo, S.; Yu, J.; Yu, S.; Sun, R.; Cao, L.; Liao, W. H.; Wong, C. P. Significantly enhanced electrostatic energy storage performance of flexible polymer composites by introducing highly insulating-ferroelectric microhybrids as fillers. *Adv Energy Mater.* **2019**, *9*, 1803204.

(7) Li, Q.; Chen, L.; Gadinski, M. R.; Zhang, S.; Zhang, G.; Li, H. Y.; Iagodkine, E.; Haque, A.; Chen, L. Q.; Jackson, T.; Wang, Q. Flexible high-temperature dielectric materials from polymer nanocomposites. *Nature* **2015**, *523*, 576-579.

(8) Chen, J.; Wang, Y.; Yuan, Q.; Xu, X.; Niu, Y.; Wang, Q.; Wang, H. Multilayered ferroelectric polymer films incorporating low-dielectric constant components for concurrent enhancement of energy density and charge–discharge efficiency. *Nano Energy* **2018**, *54*, 288-296.

(9) Li, L.; Feng, R.; Zhang, Y.; Dong, L. Flexible, transparent and high dielectric-constant fluoropolymer-based nanocomposites with a fluoride-constructed interfacial structure. *J. Mater. Chem. C* **2017**, *5*, 11403-11410.

(10) Li, W.; Meng, Q.; Zheng, Y.; Zhang, Z.; Xia, W.; Xu, Z. Electric energy storage properties of poly (vinylidene fluoride). *Appl. Phys. Lett.* **2010**, *96*, 192905.

(11) Cao, Y.; Irwin, P.C.; Younsi, K. The future of nanodielectrics in the electrical power industry. *IEEE Trans. Dielectr. Electr. Insul.* **2004**, *11*, 797-807.

(12) Zhou, Y.; Li, Q.; Dang, B.; Yang, Y.; Shao, T.; Li, H.; Hu, J.; Zeng, R.; He, J.; Wang, Q. A scalable, high-throughput, and environmentally benign approach to polymer dielectrics exhibiting significantly improved capacitive performance at high temperatures. *Adv. Mater.* **2018**, *30*, 1805672.

(13) Rabuffi, M.; Picci, G. Status quo and future prospects for metallized polypropylene energy storage capacitors. *IEEE Trans. Plasma Sci.* **2002**, *30*, 1939-1942.

(14) Jin, L.; Li, F.; Zhang, S. Decoding the fingerprint of ferroelectric loops: comprehension of the material properties and structures. *J. Am. Ceram. Soc.* **2014**, *97*, 1-27.

(15) Fan, B.; Liu, F.; Yang, G.; Li, H.; Zhang, G.; Jiang, S.; Wang, Q. Dielectric materials for high-temperature capacitors. *IET Nanodielectr.* **2018**, *1*, 32-40.

(16) Wei, J.; Zhu, L. Intrinsic polymer dielectrics for high energy density and low loss electric energy storage. *Prog. Polym. Sci.* **2020**, *106*, 101254.

(17) Li, Q.; Yao, F. Z.; Liu, Y.; Zhang, G.; Wang, H.; Wang, Q. High-temperature dielectric materials for electrical energy storage. *Annu. Rev. Mater. Res.* **2018**, *48*, 219-243.

(18) Dang, Z. M.; Yao, S. H.; Yuan, J. K.; Bai, J. Tailored dielectric properties based on microstructure change in $BaTiO_3$-carbon nanotube/polyvinylidene fluoride three-phase nanocomposites. *J. Phys. Chem. C* **2010**, *114*, 13204-13209.

(19) Dang, Z. M.; Zheng, M. S.; Zha, J. W. 1D/2D carbon nanomaterial-polymer dielectric composites with high permittivity for power energy storage applications. *Small* **2016**, *12*, 1688-1701.

(20) Zhang, Q.; Zhang, Z.; Xu, N.; Yang, H. Dielectric properties of P (VDF-TrFE-CTFE) composites filled with surface-coated TiO_2 nanowires by SnO_2 nanoparticles. *Polymers* **2020**, *12*, 85.

(21) Xie, Y.; Jiang, W.; Fu, T.; Liu, J.; Zhang, Z.; Wang, S. Achieving high energy density and low loss in PVDF/BST nanodielectrics with enhanced structural homogeneity. *ACS Appl. Mater. Interfaces* **2018**, *10*, 29038-29047.

(22) Zheng, M. S.; Zheng, Y. T.; Zha, J. W.; Yang, Y.; Han, P.; Wen, Y. Q.; Dang, Z. M. Improved dielectric, tensile and energy storage properties of surface rubberized $BaTiO_3$/polypropylene nanocomposites. *Nano Energy* **2018**, *48*, 144-151.

(23) Luo, S.; Yu, S.; Sun, R.; Wong, C. P. Nano Ag-deposited $BaTiO_3$ hybrid particles as fillers for polymeric dielectric composites: toward high dielectric constant and suppressed loss. *ACS Appl. Mater. Interfaces* **2014**, *6*, 176-182.

(24) Zhang, L.; Wang, Y.; Xu, M.; Wei, W.; Deng, Y. Multiple interfacial modifications in poly (vinylidene fluoride)/barium titanate nanocomposites via double-shell architecture for significantly enhanced energy storage density. *ACS Appl. Energy Mater.* **2019**, *2*, 5945-5953.

(25) Huang, Y.; Huang, X.; Schadler, L. S.; He, J.; Jiang, P. Core@double-shell structured nanocomposites: a route to high dielectric constant and low loss material. *ACS Appl. Mater. Interfaces* **2016**, *8*, 25496-25507.

(26) Zhu, M.; Huang, X.; Yang, K.; Zhai, X.; Zhang, J.; He, J.; Jiang, P. Energy storage in ferroelectric polymer nanocomposites filled with core–shell structured polymer@$BaTiO_3$ nanoparticles: understanding the role of polymer shells in the interfacial regions. *ACS Appl. Mater. Interfaces* **2014**, *6*, 19644-19654.

(27) Chi, Q. G.; Dong, J. F.; Zhang, C. H.; Wong, C. P.; Wang, X.; Lei, Q. Q. Nano iron oxide-deposited calcium copper titanate/polyimide hybrid films induced by an external magnetic field: toward a high dielectric constant and suppressed loss. *J. Mater. Chem. C* **2016**, *4*, 8179-8188.

(28) Li, Z.; Liu, F.; Yang, G.; Li, H.; Dong, L.; Xiong, C.; Wang, Q. Enhanced energy storage performance of ferroelectric polymer nanocomposites at relatively low electric fields induced by surface modified $BaTiO_3$ nanofibers. *Compos. Sci. Technol.* **2018**, *164*, 214-221.

(29) Lu, X.; Zou, X.; Shen, J.; Zhang, L.; Jin, L.; Cheng, Z. Y. High energy density with ultrahigh discharging efficiency obtained in ceramic-polymer nanocomposites using a non-ferroelectric polar polymer as matrix. *Nano Energy* **2020**, *70*, 104551.

(30) Sun, W.; Lu, X.; Jiang, J.; Zhang, X.; Hu, P.; Li, M.; Lin, Y. H.; Nan, C. W.; Shen, Y. Dielectric and energy storage performances of polyimide/$BaTiO_3$ nanocomposites at elevated temperatures. *J. Appl. Phys.* **2017**, *121*, 244101.

(31) Zhang, G.; Brannum, D.; Dong, D.; Tang, L.; Allahyarov, E.; Tang, S.; Kodweis, K.; Lee, J. K.; Zhu, L. Interfacial polarization-induced loss mechanisms in polypropylene/$BaTiO_3$ nanocomposite dielectrics. *Chem. Mater.* **2016**, *28*, 4646-4660.

(32) Zhou, Y.; Yuan, C.; Wang, S.; Zhu, Y.; Cheng, S.; Yang, X.; Yang, Y.; Hu, J.; He J.; Li, Q. Interface-modulated nanocomposites based on polypropylene for high-temperature energy storage. *Energy Storage Mater.* **2020**, *28*, 255-263.

(33) Ai, D.; Li, H.; Zhou, Y.; Ren, L.; Han, Z.; Yao, B.; Zhou, W.; Zhao, L.; Xu, J.; Wang, Q. Tuning nanofillers in in situ prepared polyimide nanocomposites for high-temperature capacitive energy storage. *Adv. Energy Mater.* **2020**, *10*, 1903881.

(34) Wang, W.; Min, D.; Li, S. Understanding the conduction and breakdown properties of polyethylene nanodielectrics: effect of deep traps. *IEEE Trans. Dielectr. Electr. Insul.* **2016**, *23*, 564-572.

(35) Thakur, Y.; Lean, M. H.; Zhang, Q. M. Reducing conduction losses in high energy density polymer using nanocomposites. *Appl. Phys. Lett.* **2017**, *110*, 122905.

(36) Li, H.; Ai, D.; Ren, L.;Yao, B.; Han, Z.; Shen, Z.; Wang, J.; Chen, L. Q.; Wang, Q. Scalable polymer nanocomposites with record high-temperature capacitive performance enabled by rationally designed nanostructured inorganic fillers. *Adv. Mater.* **2019**, *31*, 1900875.

(37) Samant, S. P.; Grabowski, C. A.; Kisslinger, K.; Yager, K. G.; Yuan, G.; Satija, S. K.; Durstock, M. F.; Raghavan, D.; Karim, A. Directed self-assembly of block copolymers for high breakdown strength polymer film capacitors. *ACS Appl. Mater. Interfaces* **2016**, *8*, 7966-7976.

(38) Wang, Y.; Chen, J.; Li, Y.; Niu, Y.; Wang, Q.; Wang, H. Multilayered hierarchical polymer composites for high energy density capacitors. *J. Mater. Chem. A* **2019**, *7*, 2965-2980.

(39) Jiang, J.; Zhang, X.; Dan, Z.; Ma, J.; Lin, Y.; Li, M.; Nan, C. W.; Shen, Y. Tuning phase composition of polymer nanocomposites toward high energy density and high discharge efficiency by nonequilibrium processing. *ACS Appl. Mater. Interfaces*, **2017**, *9*, 29717-29731.

(40) Huang, H.; Chen, X.; Yin, K.; Treufeld, I.; Schuele, D. E.; Ponting, M.; Langhe, D.; Baer, E.; Zhu, L. Reduction of ionic conduction loss in multilayer dielectric films by immobilizing impurity ions in high glass transition temperature polymer layers. *ACS Appl. Energy Mater.* **2018**, *1*, 775-782.

(41) Jiang, Y.; Zhang, X.; Shen, Z.; Li, X.; Yan, J.; Li, B. W.; Nan, C. W. Ultrahigh breakdown strength and improved energy density of polymer nanocomposites with gradient distribution of ceramic nanoparticles. *Adv. Funct. Mater.* **2020**, *30*, 1906112.

(42) Li, Z.; Liu, F.; Li, H.; Ren, L.; Dong, L.; Xiong, C.; Wang, Q. Largely enhanced energy storage performance of sandwich-structured polymer nanocomposites with synergistic inorganic nanowires. *Ceram. Int.* **2019**, *45*, 8216-8221.

(43) Pan, Z.; Liu, B.; Zhai, J.; Yao, L.; Yang, K.; Shen, B. $NaNbO_3$ two-dimensional platelets induced highly energy storage density in trilayered architecture composites. *Nano Energy* **2017**, *40*, 587-595.

(44) Zhang, Y.; Chi, Q. G.; Liu, L. Z.; Zhang, T. D.; Zhang, C. H.; Chen, Q. G.; Wang, X.; Lei, Q. Q. PVDF-based dielectric composite films with excellent energy storage performances by design of nanofibers composition gradient structure. *ACS Appl. Energy Mater.* **2018**, *1*, 6320-6329.

(45) Wang, Y.; Cui, J.; Wang, L.; Yuan, Q.; Niu, Y.; Chen, J.; Wang Q.; Wang, H. Compositional tailoring effect on electric field distribution for significantly enhanced breakdown strength and restrained conductive loss in sandwich-structured ceramic. *J. Mater. Chem. A* **2017**, 5, 4710-4718.

(46) Xie, B.; Zhang, Q.; Zhang, L.; Zhu, Y.; Guo, X.; Fan, P.; Zhang, H. Ultrahigh discharged energy density in polymer nanocomposites by designing linear/ferroelectric bilayer heterostructure. *Nano Energy* **2018**, *54*, 437-446.

(47) Liu, F.; Li, Q.; Cui, J.; Li, Z.; Yang, G.; Liu, Y.; Dong, L.; Xiong, C.; Wang, H.; Wang, Q. High-energy-density dielectric polymer nanocomposites with trilayered architecture. *Adv. Funct. Mater.* **2017**, *27*, 1606292.

(48) Wang, Y.; Li, Y.; Wang, L.; Yuan, Q.; Chen, J.; Niu, Y.; Xu, X.; Wang, Q.; Wang, H. Gradient-layered polymer nanocomposites with significantly improved insulation performance for dielectric energy storage. *Energy Storage Mater.* **2020**, *24*, 626-634.

(49) Kaya, C.; He, J. Y.; Gu, X.; Butler, E. G. Nanostructured ceramic powders by hydrothermal synthesis and their applications. *Microporous Mesoporous Mater.* **2002**, *54*, 37-49.

(50) Li, H.; Ren, L.; Ai, D.; Han, Z.; Liu, Y.; Yao, B.; Wang, Q. Ternary polymer nanocomposites with concurrently enhanced dielectric constant and breakdown strength for high-temperature electrostatic capacitors. *InfoMat* **2020**, *2*, 389-400.

(51) Shen, Z. H.; Shen, Y.; Cheng, X. X.; Liu, H. X.; Chen, L. Q.; Nan, C. W. High-throughput data-driven interface design of high-energy-density polymer nanocomposites. *J. Materiomics* **2020**, *6*, 573-581.

(52) Luo, H.; Zhou, X.; Ellingford, C.; Zhang, Y.; Chen, S.; Zhou, K.; Zhang, D.; Bowen, C.R.; Wan, C. Interface design for high energy density polymer nanocomposites. *Chem. Soc. Rev.* **2019**, *48*, 4424-4465.

(53) Bao, Z.; Hou, C.; Shen, Z.; Sun, H.; Zhang, G.; Luo, Z.; Dai, Z.; Wang, C.; Chen, X.; Li, L.; Yin, Y.; Shen, Y.; Li, X. Negatively charged nanosheets significantly enhance the energy-storage capability of polymer-based nanocomposites. *Adv. Mater.* **2020**, *32*, 1907227.

(54) Liu, B.; Yang, M.; Zhou, W. Y.; Cai, H. W.; Zhong, S. L.; Zheng, M. S.; Dang, Z. M. High energy density and discharge efficiency polypropylene nanocomposites for potential high-power capacitor. *Energy Storage Mater.* **2020**, *27*, 443-452.

(55) Tomer, V.; Polizos, G.; Randall, C. A.; Manias, E. Polyethylene nanocomposite dielectrics: implications of nanofiller orientation on high field properties and energy storage. *J. Appl. Phys.* **2011**, *109*, 074113.

(56) Liu, J.; Zhang, Y.; Wang, Z.; Ding, J.; Yu, S.; Zhang, Y.; Jiang, Z. Optimizing electric field distribution via tuning cross-linked point size for improving the dielectric properties of polymer nanocomposites. *Nanoscale* **2020**, *12*, 12416-12425.

(57) J. Robertson. Band offsets of wide-band-gap oxides and implications for future electronic devices, *J. Vac. Sci. Technol. B* **2000**, *18*, 1785-1791.

(58) Chen, L.; Batra, R.; Ranganathan, R.; Sotzing, G.; Cao, Y.; Ramprasad, R. Electronic structure of polymer dielectrics: the role of chemical and morphological complexity. *Chem. Mater.* **2018**, *30*, 7699-7706.

TOC GRAPHIC

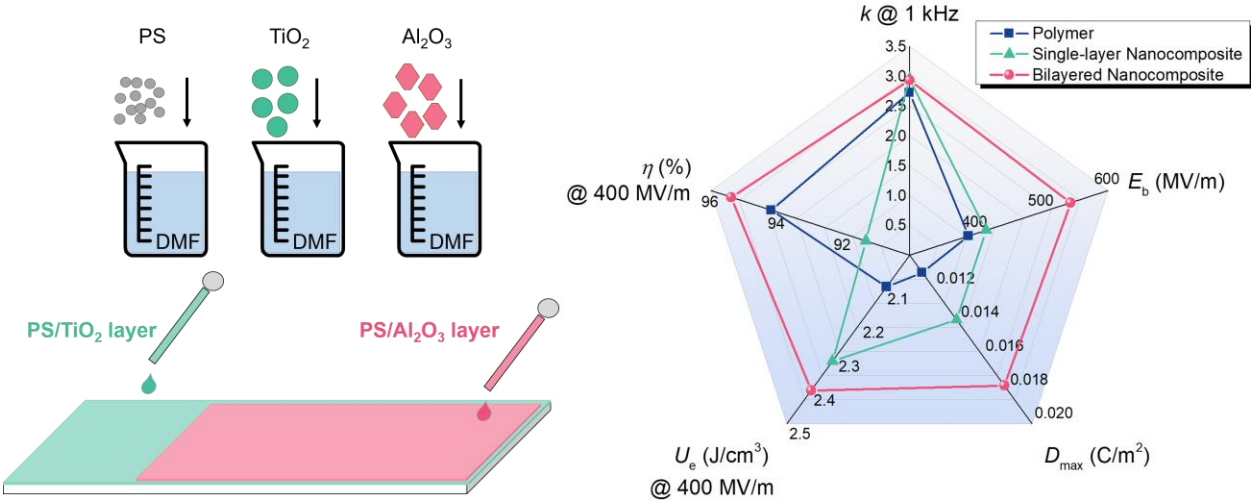
PS
TiO2
Al2O3
DMF
DMF
DMF
PS/TiO2 layer
PS/Al2O3 layer
k @ 1 kHz
Polymer
Single-layer Nanocomposite
Bilayered Nanocomposite
3.5
3.0
2.5
2.0
1.5
1.0
0.5
η (%)
@ 400 MV/m
96
94
92
600
500
400
Eb (MV/m)
0.012
0.014
0.016
0.018
0.020
Dmax (C/m2)
2.1
2.2
2.3
2.4
2.5
Ue (J/cm3)
@ 400 MV/m